ACS APPLIED NANO MATERIALS

www.acsanm.org Article

Photoreduction-Insensitive GO/rGO Patterning Based on Multistep Femtosecond Laser Writing for Implementing Fresnel Zone Plates

Shiru Jiang, Chul-Soon Park, Woo-Bin Lee, and Sang-Shin Lee*

Cite This: *ACS Appl. Nano Mater.* 2021, 4, 9283–9292 Read Online

ACCESS | Metrics & More | Article Recommendations

ABSTRACT: As boosting the degree of photoreduction widens a patterning linewidth, devices comprising femtosecond laser (fs-laser)-induced reduced graphene oxide (rGO) present the dilemma of a choice between optimum performance and miniaturization. Here, by exploiting multistep fs-laser writing with a low repetition rate, photoreduction-insensitive GO/rGO patterning is realized, which exhibits a photoreduction-insensitive and constant patterning linewidth at arbitrary stages of the evolving photoreduction process. During a photoreduction-insensitive patterning, a GO film is exposed iteratively to the same fs-laser beam to achieve targeted photoreduction levels, while the minimum patterning linewidth is preserved under a fixed pulse energy. The proposed patterning approach that results from preventing a thermal accumulation and roughening a GO/rGO surface achieves an optimizable device performance, without compromising on the feature size. In particular, a photoreduction-insensitive patterning provides a high optical transmission contrast while preserving a minimum linewidth. When two Fresnel zone plates that involve binary zones comprising GO/rGO are fabricated via single-exposure and multistep fs-laser-writing methods, respectively, the latter patterning approach provides a 3.9-fold enhancement of focusing efficiency compared with the former. Consequently, the demonstrated photoreduction-insensitive patterning approach confirms the feasibility of maintaining a patterning linewidth while tailoring the photoreduction levels of GO/rGO, thus promoting the development of GO/rGO-related micro/nanodevices.

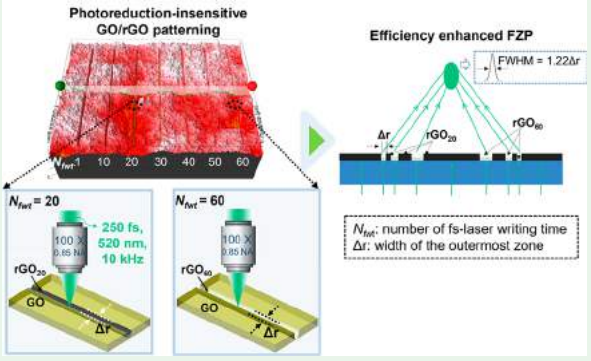

KEYWORDS: *reduced graphene oxide, preserved patterning linewidth, tunable photoreduction, femtosecond laser, photoreduction-insensitive patterning*

1. INTRODUCTION

Femtosecond laser (fs-laser)-induced micro/nanopatterning of reduced graphene oxide (rGO), accompanying in situ photoreductions, has garnered considerable attention because its properties can be effectively adjusted using a facile and maskless method.[1−5] GO/rGO-based micro/nanostructures with mechanical flexibility, chemical/physical stability, and optical and electrical property tunability have been used in various applications, such as diffractive lenses, supercapacitors, photodetectors, and actuators.[2,6−12] With the removal of oxygen and carbon atoms, the patterning linewidth and photoreduction degree of GO/rGO are adjustable by controlling the fs-laser parameters encompassing the pulse energy and repetition rate.[6,12−15] At present, the most adopted technology for the photoreduction of GO via an fs-laser is direct writing based on a single-exposure process.[5] However, when this method is used for enhancing the photoreduction degrees of GO/rGO, the side effect of the corresponding patterning linewidth widening becomes too obvious to be ignored.[12−15] The co-occurrence of tailoring the patterning linewidth and degrees of photoreduction hinders the application of fs-laser-induced GO/rGO patterning.[3,12−15] When the desired optical transmission, film thickness, and electrical conductivity come from high or medium degrees of GO/rGO photoreduction, it is unreasonable to expect to employ the minimum linewidth that can only be achievable at the lowest degree of photoreduction. Thus, the feature sizes of micro/nanodevices may be much larger than the minimum linewidth, when device performances are strongly subject to the optical and electrical properties of GO/rGO. For example, high and medium degrees of GO/rGO photoreduction, corresponding to weak and strong optical absorptions, are optimal for transparent conductors[16] and photothermal actuators,[12] respectively. However, an optical absorption may not be flexibly controlled independently of the miniaturization

Received: July 5, 2021
Accepted: August 24, 2021
Published: September 2, 2021

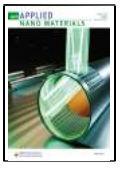

https://doi.org/10.1021/acsanm.1c01807
ACS Appl. Nano Mater. 2021, 4, 9283–9292

of a patterning linewidth, which requires a low degree of photoreduction. Regarding optical lenses, the desired degree of photoreduction is diversified because the optical transmittance, refractive index, and film thickness of GO/rGO are strictly determined according to their design criteria.[6,14,15,17] The contradiction about the photoreduction and linewidth still exists for this kind of application, considering that all the properties of GO/rGO, including the minimum patterning linewidth, can only be adjusted synchronously as a whole. For GO/rGO-based devices that rely on the fs-laser single-exposure process, the performance can only be ameliorated at the expense of feature size because the minimum patterning linewidth of GO/rGO cannot be maintained as photoreduction deviates from its lowest level.

A Fresnel zone plate (FZP) is a diffractive lens that consists of a series of concentric and alternating opaque and transparent rings.[18] Benefiting from the fs-laser-induced micro/nanopatterning of GO/rGO, FZPs provide the advantages of ultrathinness, strong focusing, and high integrability and have been frequently reported in nano-optics and on-chip photonic systems.[6,15,19,20] However, the above-mentioned concurrent variation in the degree of photoreduction and the patterning linewidth of GO/rGO leads to a trade-off between focusing resolution and efficiency.[14,15] It is known that focusing efficiency and resolution can be enhanced by attaining a distinct transmission discrepancy between adjacent binary zones and narrowing the width of the outermost zone, respectively. The radical transmission contrast generated by a high degree of photoreduction of GO contrasts with the minimum patterning linewidth under the lowest extent of photoreduction.[12−15,20] In particular, it seems rather challenging to overcome such a trade-off. For instance, although both focusing efficiency and focusing resolution are improved by applying the Rayleigh−Sommerfeld diffraction theory,[21] the trade-off between focusing resolution and efficiency still exists in the optimized lens.[15]

In this study, we propose a multistep fs-laser-writing approach for engendering a photoreduction-insensitive GO/rGO patterning, which eradicates the trade-off between focusing efficiency and resolution on FZPs. The constant patterning linewidth and tunable photoreduction presented by photoreduction-insensitive GO/rGO patterning are achieved by lowering the repetition rate to prevent a thermal accumulation and roughen the surface of GO/rGO. The number of fs-laser writing times N_{fwt} is the key to the proposed multistep fs-laser-writing method, which is differentiated from traditional direct-writing processes. With multistep fs-laser writing, the N_{fwt} can be used to control the degree of photoreduction of GO/rGO without altering the patterning linewidth, which only relies on pulse energy. This study is the first successful attempt to separately control a patterning linewidth and the degree of photoreduction of GO/rGO. The proposed patterning method provides beneficial insights into fs-laser-GO interactions and effective solutions to a performance/miniaturization trade-off in GO/rGO-based devices, such as diffractive/reflective components, supercapacitors, and photothermally actuators.

2. MATERIALS AND METHODS

2.1. Materials. Prior to the formation of GO films, glass substrates were decontaminated via an ultrasonic treatment. Adhesion between the GO solution and the substrate was promoted by applying (3-aminopropyl)triethoxysilane (99%, Sigma-Aldrich). A GO solution with a concentration of 2 mg/mL was first prepared using Hummers' method.[2] The solution was then spin-coated at 1000 rpm for 60 s and cured at 50 °C for 30 min to obtain 300 nm thick films.

2.2. Patterning Via fs-Laser. The fs-laser used in the experiment provided a pulsed beam with a wavelength, λ, of 520 nm and a duration of 250 fs, which was generated using a fundamental beam centered at λ = 1040 nm via a second harmonic generation system. The laser beam was focused on the GO surface via a 100× objective lens with a numerical aperture of 0.85, while a scanning speed of 500 μm/s was adopted for the motorized translation stage (XYCV630-C-N, Misumi). The positioning accuracy and positional repeatability of the used translation stage are 5 μm and ±0.5 μm, respectively, which causes a circular pattern to exhibit larger minimum linewidths compared with a straight line during a photoreduction-insensitive pattering. Therefore, under a threshold pulse energy of 5.7 nJ and a repetition rate of 10 kHz, the minimum linewidth for straight lines and FZPs are 0.5 and 0.8 μm, respectively. The fabrication process is elaborated in our previous work.[12]

Two FZPs, namely, FZP_{single} and $FZP_{multiple}$, were manufactured via single-exposure and multistep fs-laser writing, respectively. Otherwise, all fabrication conditions were identical. The pulse repetition rate, energy, and scanning speed adopted for the fabrication were 10 kHz, 5.7 nJ, and 500 μm/s, respectively. FZP_{single} consisted of rGO_1 and GO. The rGO_1, which was subject to single-exposure writing, was applied to form opaque zones, patterned in a sequence of concentric rings with a feature size (i.e., linewidth) of 0.8 μm. For $FZP_{multiple}$, tapping into the same concentric rings, the odd-numbered zones, corresponding to the GO regions in the case of FZP_{single}, underwent laser writing 20 times to become optically opaque, whereas the even-numbered zones became transparent when the writing process was consecutively executed 60 times.

2.3. Characterization. Three-dimensional (3D) optical profile images, which chart the depth/thickness and surface roughness of the GO/rGO films, were captured with a 3D profilometer (Profilm3D, Filmetrics). Cross-sectional images of straight rGO lines were obtained using an atomic force microscope (AFM) (XE100, PSIA). A digital optical microscope (AM-413T, Dino-Lite) and a visible−near-infrared (vis-NIR) spectrometer (USB 4000, Ocean Optics) were used to study the spectral transmission of the GO/rGO films. A scanning electron microscope (SEM) (Inspect F50, FEI) was used to characterize the surface morphology of GO/rGO. Their chemical compositions were analyzed using an X-ray photoelectron spectroscope (XPS) (K-Alpha+, ThermoFisher Scientific). The Raman spectra (FEX, NOST) were obtained using an excitation laser with a λ and power of 531 nm and 0.3 mW, respectively. The complex refractive index of rGO_1 used in the simulations was practically examined using a thin-film analyzer (F40-EXR, Filmetrics). The rGO_1 was reduced by a 10 kHz fs-laser beam with a pulse energy of 5.7 nJ. The optical response of the fabricated FZPs was inspected using a supercontinuum laser (SuperK compact, NKT Photonics), filtered through a bandpass filter centered at λ = 500 nm (FB500-10, Thorlabs). Images of the focused spot were captured using a charge-coupled device (CCD) camera (BU302MCF, Toshiba Teli) equipped with a 50× objective.

2.4. Simulations. The dependence of surface roughness on the formation of photoreduction-insensitive GO/rGO patterning was studied using simulations based on a 3D finite-difference time-domain (FDTD)-based tool (Ansys/Lumerical). A cuboid box with dimensions of 4 μm × 4 μm × 2 μm was chosen for the simulation region, whose boundaries were all set as perfectly matched layers. A pulsed Gaussian beam associated with a thin lens mode, with a pulse duration and wavelength of 250 fs and 520 nm, respectively, was normally incident on the rGO_1 film, whose thickness and complex refractive index were set to 300 nm and 1.73 + 0.09i, respectively. A thick glass was chosen as the substrate.

3. RESULTS AND DISCUSSIONS

3.1. Proposed Photoreduction-Insensitive GO/rGO Patterning. The realization of a photoreduction-insensitive

https://doi.org/10.1021/acsanm.1c01807
ACS Appl. Nano Mater. 2021, 4, 9283−9292

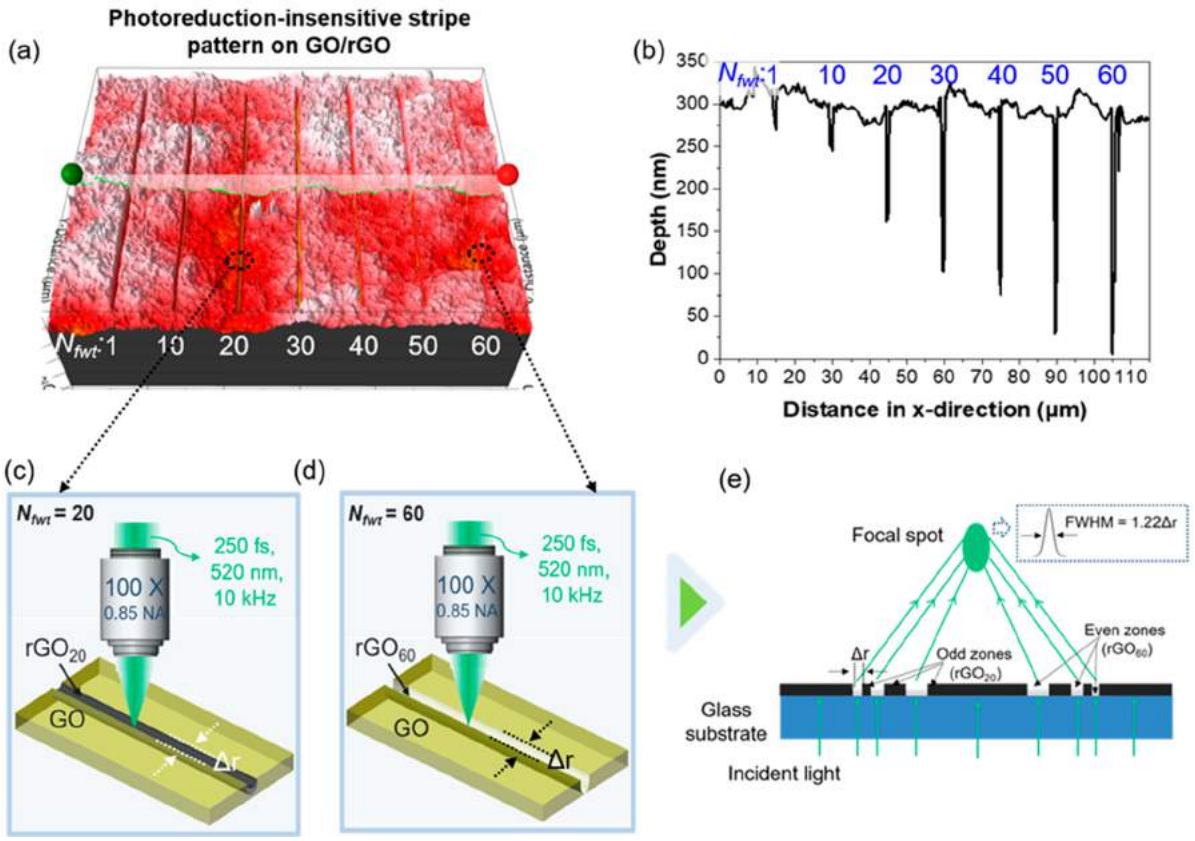

Figure 1. Illustration of photoreduction-insensitive GO/rGO patterning. (a) Surface profile image captured by a 3D optical profiler and (b) corresponding depth profiles in terms of N_{fwt}. Schematics of multistep fs-laser writing, corresponding to N_{fwt} of (c) 20 and (d) 60. (e) Schematic of the beam focusing in an FZP.

GO/rGO patterning via multistep fs-laser writing is depicted in Figure 1. Unlike fs-laser direct writing, which engages a single-exposure writing process, the proposed writing scheme tailors the N_{fwt}, rather than the parameters pertaining to the fs-laser system, to achieve the desired photoreduction. The proposed photoreduction-insensitive GO/rGO patterning method is presumed to stably preserve a small patterning linewidth due to the fixed pulse energy, while the photoreduction level is adjusted by N_{fwt} through a process of an accumulated photoreduction. When an fs-laser beam with a repetition rate of 10 kHz irradiates a 300 nm thick GO film, a photoreduction-insensitive stripe pattern, comprising a set of rGO lines, is formed, with the same linewidth under different N_{fwt}, as illustrated in Figure 1a. An adjustable photoreduction can be featured by a flexible control of the thickness and optical transmission of rGO, which is a well-established strategy for creating diffraction-based optical devices.[6,12,14,19−22] As shown in Figure 1a,b, the surface profiles measured by a 3D profilometer signify that a constant linewidth was obtained irrespective of the rGO depths, depending on the N_{fwt}. Furthermore, the optical transmission was seen to be sensitive to the degree of photoreduction and eventually directed by laser-writing treatment repetitions. In particular, rGO_{20} and rGO_{60}, which represent rGO patterns that correspond to 20 and 60 laser treatment repetitions, respectively, were considered. As plotted in Figure 1c, rGO_{20} gave rise to a lower transmission than its GO counterpart with no laser exposure. However, rGO_{60} as displayed in Figure 1d, provided a higher transmission across the entire visible spectral region than GO, while the linewidths of rGO_{20} and rGO_{60} were almost equivalent. The patterning depth and optical transmission of rGO films are primarily attributed to the detachment of oxygen and carbon atoms during repeated fs-laser-writing treatments.[2,20]

Considering that the linewidth and degree of photoreduction were strongly related to pulse energy and N_{fwt}, respectively, by virtue of the multistep fs-laser writing, the photoreduction level of photoreduction-insensitive patterns on the GO/rGO surface could be controlled without affecting the linewidth. This implies that the minimum patterning linewidth of GO/rGO may remain approximately the same, even though its electrical, optical, and thermal properties vary in accordance with the degree of photoreduction. Therefore, a photoreduction-insensitive GO/rGO patterning can potentially provide an effective solution to the contradiction between promoting performance and miniaturizing feature size for various GO/rGO-based photothermal and optoelectronic devices.[6−12] Serving as a practical example, an FZP based on the proposed photoreduction-insensitive GO/rGO patterning approach is displayed in Figure 1e. The rGO_{20} and rGO_{60}, which are described in Figure 1c,d, are incorporated in odd- and even-numbered zones of FZP with the intention of blocking and transmitting the incident light wave, respectively. Therefore, the trade-off in FZPs between focusing efficiency and focusing resolution, which is characterized by the full width at half-maximum (FWHM), can be overcome by obtaining a high transmission contrast while preserving the minimum patterning linewidth during a photoreduction-insensitive GO/rGO patterning. Note that the width of the outermost zone (Δr), which governs the focusing resolution, is

https://doi.org/10.1021/acsanm.1c01807
ACS Appl. Nano Mater. 2021, 4, 9283−9292

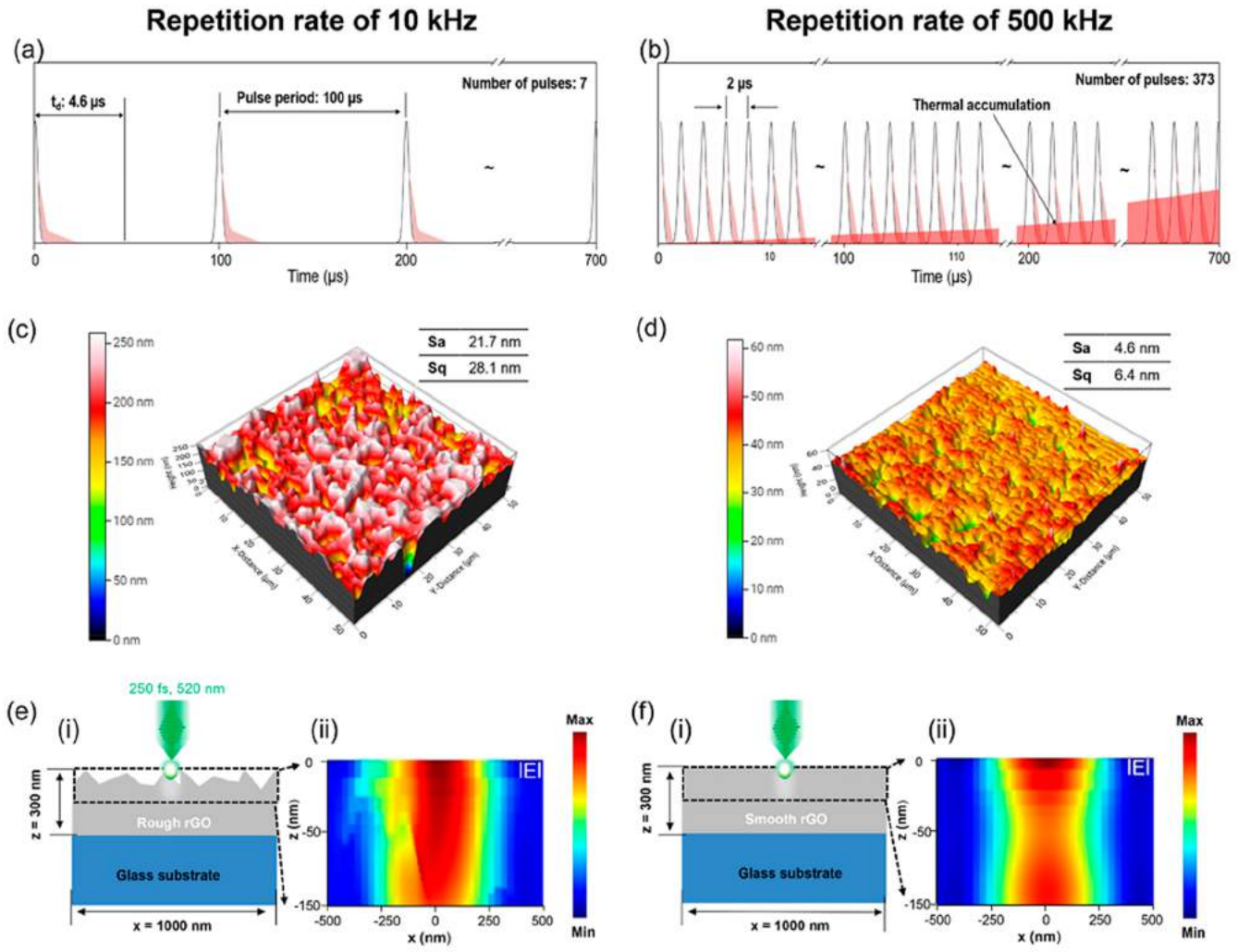

Figure 2. Examination of a thermal accumulation and surface roughness under repetition rates of 10 and 500 kHz. (a, b) Schematics of thermal accumulation induced by fs-laser pulses (shaded areas indicate a thermal accumulation). (c, d) Images of rGO_1 surface roughness obtained using a 3D profilometer. Simulated E-field distributions for (e) rough and (f) smooth rGO_1 surfaces.

equal to the patterning linewidth of rGO_1 (N_{fwt} = 1), rGO_{20}, and rGO_{60}, although their photoreduction levels are evidently different.

3.2. Theoretical Analyses and Simulation. The corresponding relationship between patterning linewidth and photoreduction degree in a conventional fs-laser direct writing was eliminated after focusing on the N_{fwt} and repetition rate, where the repetition rate is mainly responsible for a heat accumulation and rGO surface roughness. The thermal accumulation was drastically suppressed by lowering the repetition rate,[22,23] which was desirable for preserving a small linewidth. It is known that a thermal diffusion within GO/rGO films is governed by the diffusion time $t_d = \pi\omega^2/\alpha$, according to the Gaussian hotspot diffusion equation.[24] Here, ω is the radius of the laser beam, and α represents the in-plane thermal diffusivity, which can vary from 24 to 381 mm^2/s depending on the reduction levels from GO to rGO.[25] The maximum t_d in our experiment was calculated to be 4.6 μs, which was shorter than the pulse period at a repetition rate of 10 kHz. Figure 2a shows no sign of a thermal accumulation because the heat generated by one pulse dissipated prior to the arrival of the following pulse. For the 500 kHz case, the pulse period (2 μs) was shorter than t_d, invoking the thermal accumulation that is indicated by the shaded areas in Figure 2b. Whereas the photoreduction in the 10 kHz case was fulfilled by the individual pulses, in the 500 kHz case, the transition from GO to rGO stemmed from the accumulation of thermal energy, which expedited a thermal diffusion beyond the boundaries of the focal volume, widening the patterning linewidth.

Furthermore, a lower repetition rate led to a higher surface roughness, which helped the fs-laser beam propagate deeper, and induced an additional photoreduction below the surface of the rGO_1. As portrayed in Figure 2c,d, it was revealed with the aid of a 3D profilometer that, for the case of the rGO_1 film, the average roughness (Sa) and root-mean-square roughness (Sq) were larger under a repetition rate of 10 kHz than at 500 kHz. The surface roughness of rGO_1 was dependent on the spatial pulse density, defined as the number of pulses per laser beam spot,[26] which is determined by the repetition rate. After being focused on a GO film surface, the two laser beams exhibited identical spot sizes, which were determined by the laser wavelength and numerical aperture of the objective lens. The discrepancy in pulse density between repetition rates of 10 and 500 kHz was considerable in view of the corresponding numbers of pulses that amounted to 7 and 373 in Figure 2a,b,

https://doi.org/10.1021/acsanm.1c01807
ACS Appl. Nano Mater. 2021, 4, 9283−9292

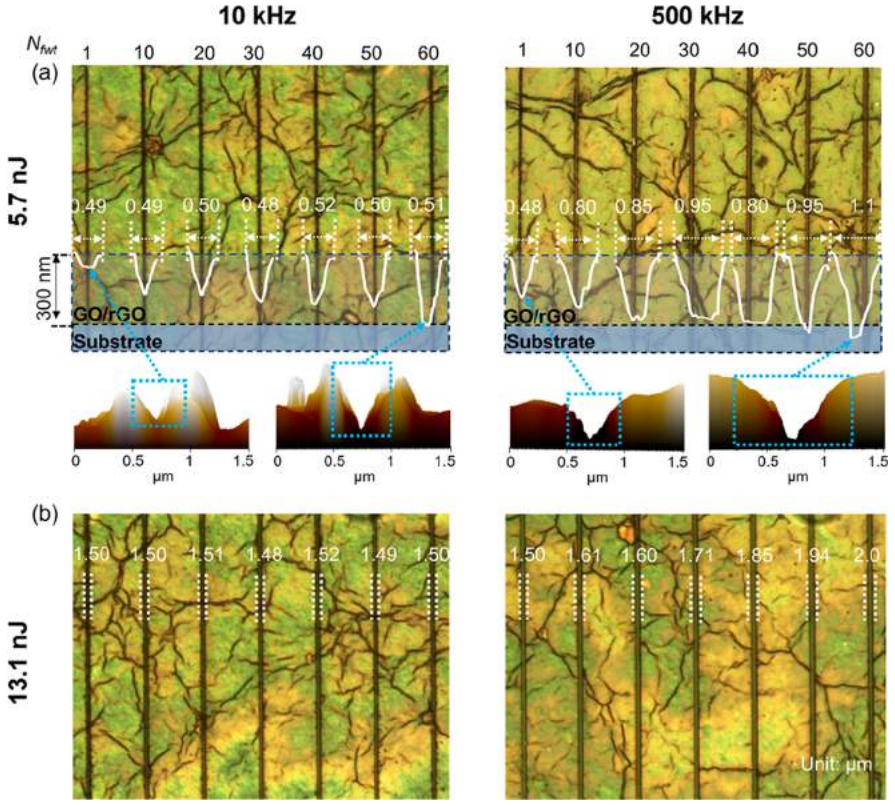

Figure 3. Microscope images of straight rGO lines patterned by multistep fs-laser writing for pulse energies of (a) 5.7 and (b) 13.1 nJ, corresponding to repetition rates of 10 and 500 kHz, respectively. Insets of (a): cross-sectional images of rGO lines measured with an AFM.

respectively, under a fixed scanning speed of 500 μm/s. A rougher rGO_1 surface was induced by a 10 kHz laser beam as a result of sparser pulse density.

To explore the influence of surface roughness on photoreduction-insensitive GO/rGO patterning, simulations were conducted using an FDTD method-based tool to determine the electric (E-) field distribution of laser beams absorbed by rGO. The fs-laser beam was simulated using a pulsed Gaussian beam that exhibited a pulse duration and wavelength of 250 fs and 520 nm, respectively. Because the photoreduction of GO/rGO is a complicated process entailing multiple physical mechanisms, a semiphenomenological theoretical model focused on optical absorption was adopted for our simulations. Assuming that the smooth rectangular rGO structure atop a SiO_2 substrate was replaced with a rough-surfaced version, as displayed in Figure 2e,f, the E-field distribution was extended below the air−rGO_1 interface. The simulation results indicated that a higher surface roughness helped guide the incident-focused laser beam to propagate deeper into the rGO_1 normal to its surface as shown in Figure 2e(ii), instead of remaining persistently around the air−rGO_1 interface. It is known that the surface roughness of a thin-film structure strongly affects the light trapping and excitation of free electrons[8,27] under a laser irradiation, which is speculated to be responsible for the surface-roughness-dependent E-field distributions of rGO_1 films. As a result, with the aid of an impinging fs-laser beam at a fixed repetition rate of 10 kHz, extra rGO was subsequently produced underneath the rGO_1 in accordance with the E-field distribution associated with the laser beam, which could not significantly widen the original linewidth existing on the air−rGO_1 interface. Therefore, the patterning linewidth of rGO_1 was retained at its initial value and transferred to subsequent rGOs with higher degrees of photoreduction after the N_{fwt} was increased. Meanwhile, for the 500 kHz case, the linewidth was unavoidably widened in accordance with laser-writing repetitions, which was attributable to the absorption of laser beams in the vicinity of the rGO_1 surface, as shown in Figure 2f(ii). Consequently, when N_{fwt} is increased, the roughened GO/rGO surface helps maintain the patterning linewidth that is determined by a single-exposure fs-laser treatment. Moreover, the repetition rate used for multistep fs-laser writing should preferably be lowered to enable a photoreduction-insensitive GO/rGO patterning.

3.3. Preserved Linewidth of GO/rGO Patterns. To ascertain the influence of repetition rate and pulse energy on the patterning linewidth of GO/rGO patterned by multistep fs-laser writing, straight lines were engraved on a GO surface. The microscope images obtained under a repetition rate of 10 kHz that are shown in Figure 3 indicate that a constant linewidth was maintained when N_{fwt} was altered; however, the linewidth began to increase upon changing N_{fwt} from 1 to 10 in the 500 kHz case. At a repetition rate of 10 kHz, the patterning linewidth was predominantly determined by pulse energy. Under a threshold pulse energy of 5.7 nJ, the minimum linewidth of 0.5 μm was preserved for the 10 kHz case, as shown in the AFM cross-sectional images in the insets of Figure 3a. Considering that the linewidth along with the patterning depth was dependent on both the pulse energy and N_{fwt} for the 500 kHz case, a low repetition rate was crucial for realizing the photoreduction-insensitive GO/rGO patterning via the proposed fs-laser-writing scheme. The dependence of the linewidth on the pulse energy was also shown.

https://doi.org/10.1021/acsanm.1c01807
ACS Appl. Nano Mater. 2021, 4, 9283−9292

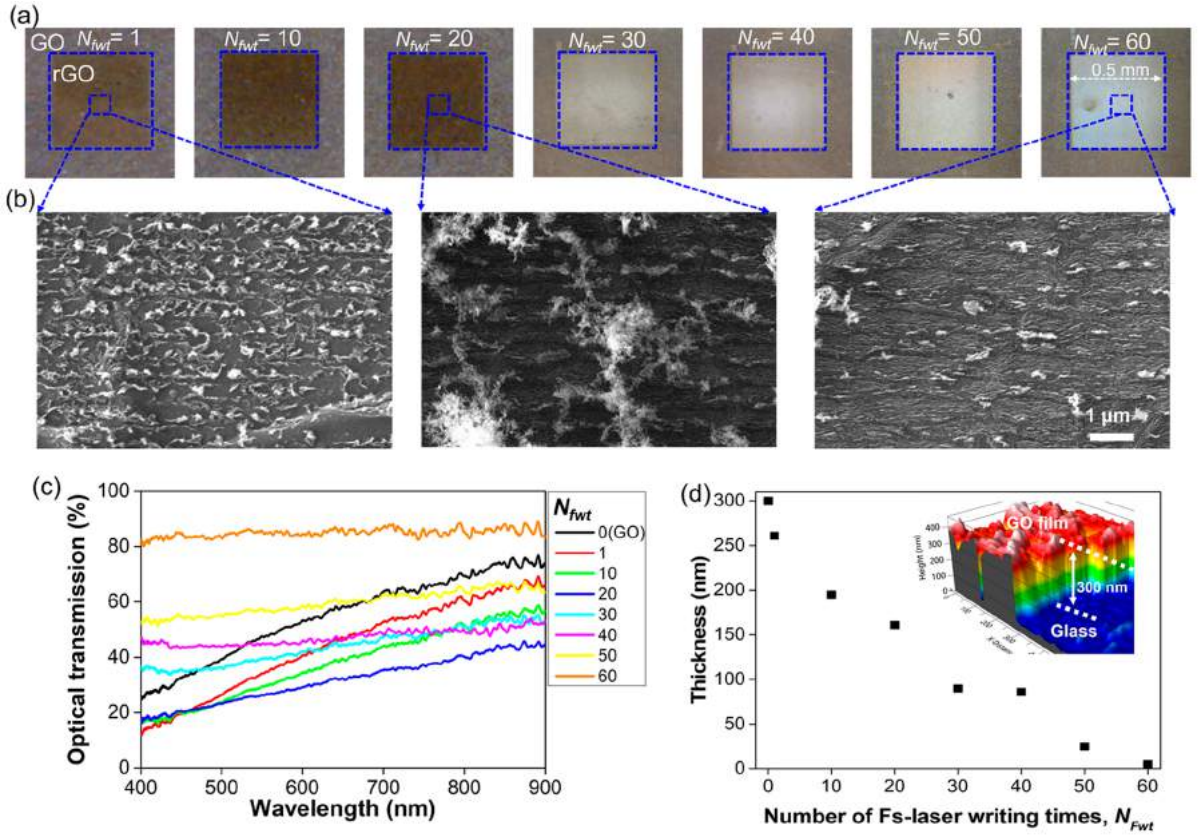

Figure 4. (a) Photographs, (b) SEM images, (c) optical transmission spectra, and (d) thicknesses of rGO films after a photoreduction-insensitive patterning using multistep fs-laser writing as a function of N_{fwt}. Inset in (d): 3D optical profile image of the prepared GO film on a glass substrate with an average thickness of ∼300 nm.

3.4. Adjustable Photoreduction of GO/rGO Patterns.

The tunable photoreduction of a photoreduction-insensitive GO/rGO patterning could be underpinned by a tailorable optical transmission and variable thickness, depending on fs-laser-writing repetitions. As depicted in Figure 4a, when N_{fwt} is increased from 1 to 60, the color contrast between GO and rGO that was observed using a digital microscope signified the differing degrees of photoreduction. The GO/rGO patterns (0.5×0.5 mm^2) were inscribed under a pulse repetition rate of 10 kHz and pulse energy of 5.7 nJ, and their observed surface morphologies are displayed in Figure 4b. Additional intermediate levels could be accessed by more finely tuning the N_{fwt}. Optical transmission spectra with respect to N_{fwt} are plotted in Figure 4c with the help of a vis-NIR spectrometer. Overall, the optical transmission initially decreases relative to pristine GO prior to increasing, with the introduction of additional fs-laser-writing treatments. Hence, the scheme of multistep fs-laser writing can circumvent the critical limitation of conventional single-exposure fs-laser direct writing. This limitation implies that the achievable minimum patterning linewidth under the direct-writing process is not compatible with a high transmission contrast within GO/rGO patterns. For example, as long as the minimum linewidth is secured, the difference in transmission between rGO_{20} (22%) and rGO_{60} (84%) at λ = 500 nm exceeded 60%, which was substantially higher than that between GO and rGO_1 that corresponds to single-exposure fs-laser writing. In response to increasing N_{fwt} from 1 to 20, the transmission spectra of rGO showed a similar wavelength dependence to that of GO. The tendency toward a lower transmission at shorter wavelengths was likely due to the characteristic GO absorption peaks in the ultraviolet band.[28,29] Under the threshold pulse energy, the degree of photoreduction at a lower N_{fwt} was not sufficient to completely nullify the absorption peaks. In addition, it is observed that the spectra of photoreduction-insensitive GO/rGO patterns were flattened in proportion to the N_{fwt}. At an N_{fwt} of 60, the transmission at shorter wavelengths rose considerably and eventually exhibited a featureless spectral response, as in the case of graphene.[30] As evidenced in Figure 4d, a decrease in thickness with increasing N_{fwt} proves that the thicknesses of rGO films after a photoreduction-insensitive patterning could be adjusted via photoreduction levels.

The carbon hybridization structures and chemical composition of rGO with a photoreduction-insensitive patterning were investigated via Raman spectroscopy and XPS, respectively. Carbon-based materials mostly contain structural defects due to the presence of oxygen-containing groups and the E_{2g} mode associated with the stretching motion of sp^2 carbon atoms, which correspond to the D and G peaks at wavenumbers of 1351 and 1594 cm^{-1}, respectively.[31] The two-dimensional (2D) band with a peak at ∼2700 cm^{-1}, corresponding to the second-order zone-boundary phonons, indicates the atom-stacking morphology of multilayer graphene.[32] In addition, a decrease in the D- to G-peak intensity ratio (I_D/I_G) serves as an indicator of the reduction from GO to rGO.[8] Figure 5a shows that I_D/I_G decreases from 1.054 to 0.897 between the Raman spectra of GO and rGO_{60}, implying the removal of oxygen-containing groups and the re-establishment of the sp^2 network. When the fs-laser writing was performed 60 times, the disappearance of the 2D band

https://doi.org/10.1021/acsanm.1c01807
ACS Appl. Nano Mater. 2021, 4, 9283−9292

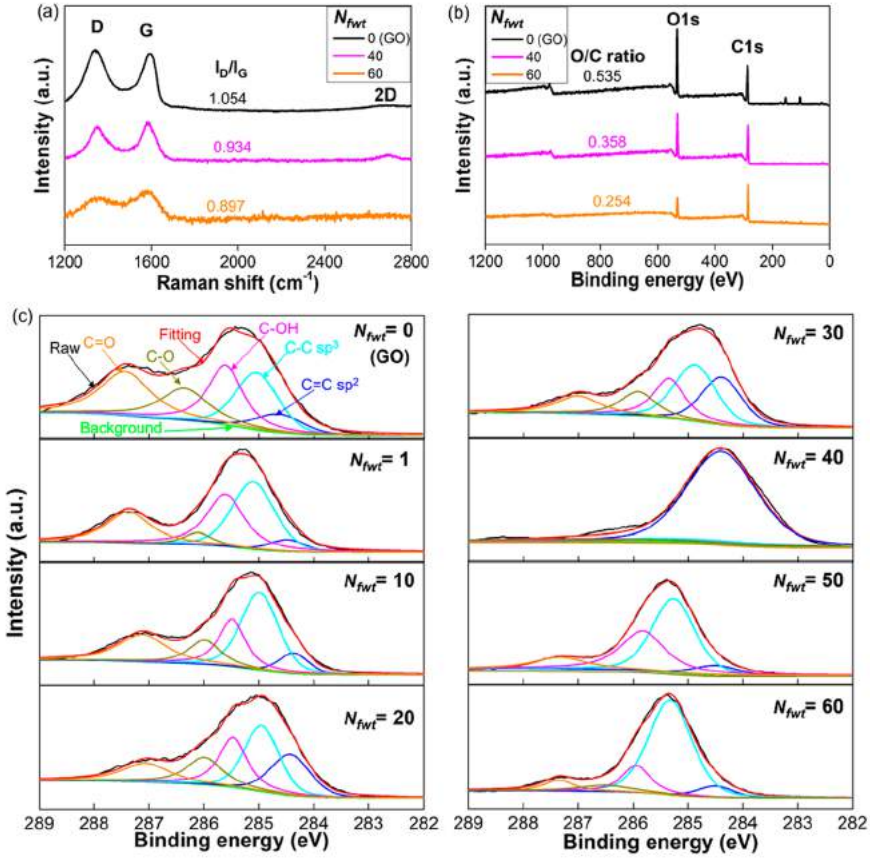

Figure 5. (a) Raman spectra, (b) XPS survey spectra, and (c) high-resolution C1s XPS spectra of rGO films involved in photoreduction-insensitive patterning with respect to N_{fwt}, for multistep fs-laser writing.

indicated that rGO_{60} was highly localized and that the graphene-like stacking morphology was destroyed, which should be attributed to severe GO/rGO ablating and fragmentation.

XPS is an effective technique for evaluating the degree of GO photoreduction via a characterization of elemental ratios of the chemical binding states on an GO/rGO film. According to the overall XPS survey spectra in Figure 5b, the decrease in the oxygen to carbon content ratio (O/C) with increased N_{fwt} indicated that oxygen atoms could be effectively eliminated from the GO surface. The high-resolution spectra of the C1s peak of GO/rGO were fitted into five component peaks: C═C sp^2 (284.5 eV), C−C sp^3 (285 eV), C−OH (285.5 eV), C−O (286.7 eV), and C═O (287.6 eV),[33,34] as displayed in Figure 5c. For the N_{fwt} = 1 case, the removal of oxygen could only be observed without the enhanced intensity of the C═C sp^2 peak, compared with pristine GO. When N_{fwt} was in the range of 1−40, the shift from sp^3 to sp^2 was clarified through the consistent increase in the sp^2 peak intensity. When N_{fwt} was further increased, the sp^2 peak intensity weakened gradually, and the C1s spectra mimicked the features of glass,[35] signifying that the photoreduction process was dictated by the ablation and etching of GO/rGO.

The demonstration of various properties of GO/rGO provided key insights into the mechanisms of photoreduction of GO, which is induced by the proposed multistep fs-laser writing. With the help of the C1s XPS spectra, when the N_{fwt} increased from 0 to 60, we could identify the three distinct subprocesses of photoreduction, including the removal of oxygen, restoration of the sp^2 carbon structure, and disappearance of the C═C sp^2 peak. At a low N_{fwt}, the optical transmission, I_D/I_G of the Raman spectra, and the O/C ratio in the XPS test showed lower values compared to those of pristine GO, signifying that oxygen functional groups were predominantly photochemically removed from the GO/rGO surface. With increasing N_{fwt} values, photoreduction mainly relied on a thermally assisted restoration of the sp^2 carbon structure, leading to the graphitization of GO and a boosted 2D peak in the Raman spectra.[36] Hence, the optical transmission started to rise with the disappearance of oxygen and carbon. For a high N_{fwt}, GO/rGO was almost ablated due to the gasification of both oxygen and carbon species in the course of repeated fs-laser irradiations. The film was extremely thinned, so that optical transmission was substantially elevated, and the Raman and C1s XPS spectra involved no 2D and C═C sp^2 peaks as in the case of the substrate. It is claimed that an effective and tunable photoreduction scheme for enabling a photoreduction-insensitive GO/rGO patterning can be achieved by managing the N_{fwt} for a multistep fs-laser writing.

3.5. Efficiency-Enhanced FZP. For typical GO/rGO-based FZPs,[14,20] which are manufactured via single-exposure fs-laser writing, there should be a trade-off between focusing efficiency and resolution. The focusing efficiency and resolution can be improved by elevating the transmission contrast between adjacent binary zones and reducing feature size, respectively.[14,15,19] A high transmission contrast may not be concurrently achieved alongside a minimized patterning linewidth of GO/rGO, from the viewpoint of photoreduction

https://doi.org/10.1021/acsanm.1c01807
ACS Appl. Nano Mater. 2021, 4, 9283−9292

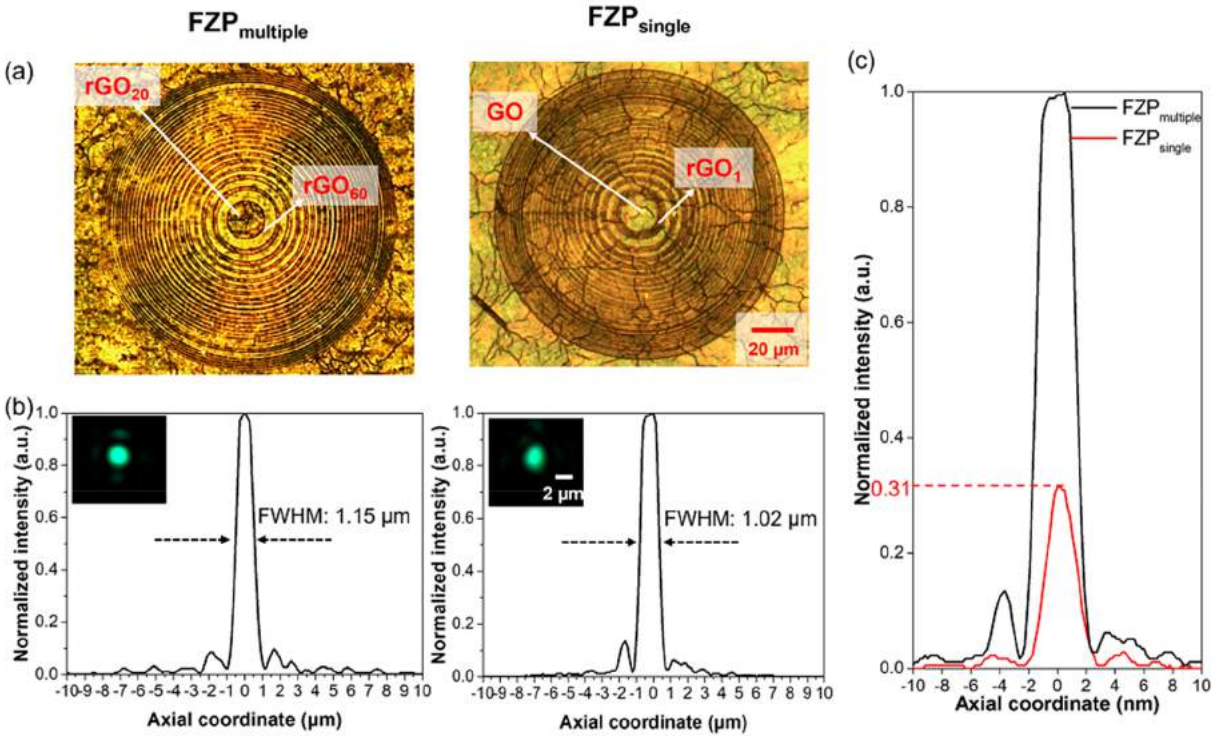

Figure 6. Characterization of $FZP_{multiple}$ and FZP_{single} fabricated via multistep and single-exposure fs-laser writing, respectively. (a) Optical microscope images and (b) intensity profiles of the focused beams (insets: captured focal spots at the focal plane) of the two FZPs in response to an illumination by a plane-wave light source with a wavelength of 500 nm. (c) Comparison of the focal spot intensities between the two FZPs.

levels.[13,14] This limitation in FZP performance can be mitigated by introducing photoreduction-insensitive GO/rGO patterning induced by fs-laser multistep writing, which allows for a miniaturized patterning linewidth as well as a high transmission contrast, with the assistance of a particular N_{fwt} and a low repetition rate of 10 kHz.

With the aim of validating the improvement in the FZP performance caused by addressing the focusing efficiency/resolution trade-off, after taking advantage of the photoreduction-insensitive GO/rGO patterning, we conducted a comparative experiment. Two different FZPs, $FZP_{multiple}$ and FZP_{single}, were designed to exhibit a diameter, focal length, and FWHM of 127 μm, 200 μm, and 1 μm, respectively, and were then fabricated using multistep and single-exposure fs-laser writing, respectively. The fabrication conditions were identical except for the N_{fwt}. Noting a transmission distinction of ~60% between rGO_{20} and rGO_{60}, which was identified at a wavelength of 500 nm, rGO_{20} and rGO_{60} were chosen for the odd and even zones of $FZP_{multiple}$, respectively. The operation wavelength for the two FZPs was correspondingly determined to be 500 nm. The minimum linewidth was inherited by both rGO_{20} and rGO_{60} from rGO_1, where the rGO_1 was also available in the single-exposure fs-laser case. As a result, the combination of rGO_1 and GO was selected to form alternating binary zones of FZP_{single} to achieve high focusing resolution; however, the corresponding transmission contrast between the binary zones is insufficient. The choice of either the odd- or even-numbered zones to be opaque is arbitrary. As shown in Figure 6a, although FZP_{single} was constructed according to reversed zone transparency characteristics compared to the $FZP_{multiple}$ and involved transparent odd zones and opaque even zones, the lens characteristics were effectively the same. The zone interfaces for $FZP_{multiple}$ seemed clearer than those for FZP_{single}, as shown in Figure 6a, implying a higher transmission contrast between the alternate zones. Figure 6b shows the intensity profiles in response to the captured images of the focal spots, revealing almost identical focusing resolutions, as estimated by FWHM values of 1.15 and 1.02 μm for $FZP_{multiple}$ and FZP_{single}, respectively. The measured focusing efficiency of $FZP_{multiple}$ was 13.1%, defined as the ratio of the power in the focal region to the total input power, and it represented an ~3.9-fold enhancement compared to that of FZP_{single} (3.4%). Figure 6c delineates the intensity profiles for the focal spots under a constant input optical power, supporting the superiority of $FZP_{multiple}$, which relies on a photoreduction-insensitive patterning for its focusing efficiency. The proposed photoreduction-insensitive GO/rGO patterning induced by a multistep fs-laser writing could maximize the transmission difference while maintaining a constant linewidth, thereby overcoming the compromise between focusing efficiency and resolution presented by current FZP devices.

4. CONCLUSION

A photoreduction-insensitive GO/rGO patterning featuring a constant patterning linewidth and tunable photoreduction levels via a multistep fs-laser writing was demonstrated in this study. A low pulse repetition rate of 10 kHz and N_{fwt}, which affects the laser pulse thermal accumulation and surface roughness of the GO/rGO film, were the crucial conditions for engendering photoreduction-insensitive patterning through multistep writing. A fixed pulse energy and variable N_{fwt} were responsible for preserving the patterning linewidth and adjustable photoreduction, respectively, which were evidenced by measured cross-sectional profiles, optical transmissions, thicknesses, and Raman and XPS spectra. The well-known

https://doi.org/10.1021/acsanm.1c01807
ACS Appl. Nano Mater. 2021, 4, 9283−9292

focusing efficiency/resolution trade-off in GO/rGO-related FZPs was overcome by utilizing the proposed photoreduction-insensitive GO/rGO patterning method. The $FZP_{multiple}$ based on a photoreduction-insensitive GO/rGO patterning exhibited a 3.9-fold enhancement in focusing efficiency compared to that of FZP_{single} fabricated by a single-exposure laser treatment, without experiencing any deterioration in the focusing resolution. The proposed photoreduction-insensitive GO/rGO patterning method demonstrates a simultaneous preservation of linewidth alongside a tunable photoreduction, indicating a great potential to mitigate the dilemma of choosing between an outstanding performance and a small feature size in micro/nanodevices that contain GO/rGO.

AUTHOR INFORMATION

Corresponding Author

Sang-Shin Lee − *Department of Electronic Engineering and Nano Device Application Center, Kwangwoon University, Seoul 01897, South Korea;* orcid.org/0000-0001-5686-4893; Email: slee@kw.ac.kr

Authors

Shiru Jiang − *Department of Electronic Engineering and Nano Device Application Center, Kwangwoon University, Seoul 01897, South Korea*

Chul-Soon Park − *Nano Device Application Center, Kwangwoon University, Seoul 01897, South Korea*

Woo-Bin Lee − *Department of Electronic Engineering and Nano Device Application Center, Kwangwoon University, Seoul 01897, South Korea*

Complete contact information is available at: https://pubs.acs.org/10.1021/acsanm.1c01807

Author Contributions

The manuscript was written through the contributions of all the authors. All authors have given their approval to the final version of the manuscript.

Notes

The authors declare no competing financial interest.

ACKNOWLEDGMENTS

This research was supported by the Basic Science Research Program offered by the National Research Foundation of Korea (NRF), funded by the Ministry of Education (No. 2018R1A6A1A03025242) and the Ministry of Science and ICT (No. 2020R1A2C3007007).

ABBREVIATIONS

GO, graphene oxide
rGO, reduced graphene oxide
fs-laser, femtosecond laser
FZP, Fresnel zone plate
N_{fwt}, the number of fs-laser writing times
SiO_2, silicon dioxide
FDTD, finite-difference time-domain
AFM, atomic force microscope
XPS, X-ray photoelectron spectroscopy
Sa, average roughness
Sq, root-mean-square roughness.

REFERENCES

(1) Jiang, H.; Zhao, B.; Liu, Y.; Li, S.; Liu, J.; Song, Y.; Wang, D.; Xin, W.; Ren, L. Review of Photoreduction and Synchronous Patterning of Graphene Oxide Toward Advanced Applications. *J. Mater. Sci.* **2020**, *55*, 480−497.

(2) Zhang, Y.; Guo, L.; Xia, H.; Chen, Q.; Feng, J.; Sun, H. Photoreduction of Graphene Oxides: Methods, Properties, and Applications. *Adv. Opt. Mater.* **2014**, *2* (1), 10−28.

(3) Fu, X.; Chen, Z.; Han, D.; Zhang, Y.; Xia, H.; Sun, H. Laser Fabrication of Graphene-Based Supercapacitors. *Photonics Res.* **2020**, *8* (4), 577−588.

(4) Jia, L.; Wu, J.; Yang, T.; Jia, B.; Moss, D. Large Third-Order Optical Kerr Nonlinearity in Nanometer-Thick $PdSe_2$ 2D Dichalcogenide Films: Implications for Nonlinear Photonic Devices. *ACS Appl. Nano Mater.* **2020**, *3* (7), 6876−6883.

(5) Liu, Y.; Mao, J.; Chen, Z.; Han, D.; Jiao, Z.; Ma, J.; Jiang, H.; Yang, H. Three-Dimensional Micropatterning of Graphene by Femtosecond Laser Direct Writing Technology. *Opt. Lett.* **2020**, *45* (1), 113−116.

(6) Lee, H.; Low, M. J.; Joel Lim, C. H.; An, J.; Sandeep, C.S. S.; Rohith, T. M.; Rhee, H.-G.; Murukeshan, V. M.; Kim, Y.-J. Transferable Ultra-Thin Multi-Level Micro-Optics Patterned by Tunable Photoreduction and Photoablation for Hybrid Optics. *Carbon* **2019**, *149*, 572−581.

(7) Sabari Girisun, T.C.; Saravanan, M.; Soma, V. R. Wavelength-Dependent Nonlinear Optical Absorption and Broadband Optical Limiting in Au-Fe_2O_3-rGO Nanocomposites. *ACS Appl. Nano Mater.* **2018**, *1* (11), 6337−6348.

(8) Zou, T.; Zhao, B.; Xin, W.; Wang, Y.; Wang, B.; Zheng, X.; Xie, H.; Zhang, Z.; Yang, J.; Guo, C. High-Speed Femtosecond Laser Plasmonic Lithography and Reduction of Graphene Oxide for Anisotropic Photoresponse. *Light: Sci. Appl.* **2020**, *9*, 69.

(9) Li, Y.; Zhang, Y.; Chen, Z.; Li, Q.; Li, T.; Li, M.; Zhao, H.; Sheng, Q.; Shi, W.; Yao, J. Self-Powered, Flexible, and Ultrabroadband Ultraviolet-Terahertz Photodetector Based on a Laser-Reduced Graphene Oxide/$CsPbBr_3$ Composite. *Photonics Res.* **2020**, *8* (8), 1301−1308.

(10) Zhu, L.; Gao, Y.; Han, B.; Liu, S.; Fu, X.; Ding, H.; Zhang, Y. Programmable Laser Patterning of Ag Nanoparticles and Reduced Graphene Oxide Hybrid Electrodes for Nonenzymatic Hydrogen Peroxide Detection. *ACS Appl. Nano Mater.* **2019**, *2* (12), 7989−7996.

(11) Li, Q.; Ding, Y.; Yang, L.; Li, L.; Wang, Y. Periodic Nanopatterning and Reduction of Graphene Oxide by Femtosecond Laser to Construct High-Performance Micro-Supercapacitors. *Carbon* **2021**, *172*, 144−153.

(12) Jiang, S.; Park, C.; Lee, W.; Zhou, C.; Lee, S. Light-Driven Diffraction Grating Based on a Photothermal Actuator Incorporating Femtosecond Laser-Induced GO/rGO. *Opt. Express* **2020**, *28* (26), 39552−39562.

(13) Ji, L.; Lee, H.; Lim, C.; Murukeshan, V.; Kim, Y. Direct Laser Writing of Graphene Oxide Patterns Using Femtosecond Laser Pulses with Different Repetition Rates. In *2017 Conference on Lasers and Electro-Optics Pacific Rim;* Optical Society of America, 2017; paper s1608.

(14) Lee, H.; Low, M.; Lim, C.; Murukeshan, V.; Kim, Y. Direct Laser Writing of Tunable Diffractive Micro-Optics on Graphene Oxide Film. *Proc. SPIE MOEMS and Miniaturized Systems XVII* **2018**, *10545*, 1054504.

(15) Zheng, X.; Jia, B.; Lin, H.; Qiu, L.; Li, D.; Gu, M. Highly Efficient and Ultra-Broadband Graphene Oxide Ultrathin Lenses with Three-Dimensional Subwavelength Focusing. *Nat. Commun.* **2015**, *6* (1), 8433.

(16) Ma, Y.; Zhi, L. Graphene-Based Transparent Conductive Films: Material Systems, Preparation and Applications. *Small Methods* **2019**, *3* (1), 1800199.

(17) Cao, G.; Lin, H.; Fraser, S.; Zheng, X.; Del Rosal, B.; Gan, Z.; Wei, S.; Gan, X.; Jia, B. Resilient Graphene Ultrathin Flat Lens in

Aerospace, Chemical, and Biological Harsh Environments. *ACS Appl. Mater. Interfaces* **2019**, *11* (22), 20298−20303.
(18) Zhang, Z.; Guo, C.; Wang, R.; Hu, H.; Zhou, X.; Liu, T.; Xue, D.; Zhang, X.; Zhang, F.; Zhang, X. Hybrid-Level Fresnel Zone Plate for Diffraction Efficiency Enhancement. *Opt. Express* **2017**, *25* (26), 33676−33687.
(19) Yang, Y.; Lin, H.; Zhang, B.; Zhang, Y.; Zheng, X.; Yu, A.; Hong, M.; Jia, B. Graphene-Based Multilayered Metamaterials with Phototunable Architecture for on-Chip Photonic Devices. *ACS Photonics* **2019**, *6* (4), 1033−1040.
(20) Low, M. J.; Lee, H.; Lim, C. H. J.; Suchand Sandeep, C.S.; Murukeshan, V. M.; Kim, S.-W.; Kim, Y.-J. Laser-Induced Reduced-Graphene-Oxide Micro-Optics Patterned by Femtosecond Laser Direct Writing. *Appl. Surf. Sci.* **2020**, *526*, 146647.
(21) Wang, Z.; Yang, T.; Zhang, Y.; Ou, Q.; Lin, H.; Zhang, Q.; Chen, H.; Hoh, H.; Jia, B.; Bao, Q. Flat Lenses Based on 2D Perovskite Nanosheets. *Adv. Mater.* **2020**, *32* (30), 2001388.
(22) Rahaman, A.; Kar, A.; Yu, X. Thermal Effects of Ultrafast Laser Interaction with Polypropylene. *Opt. Express* **2019**, *27* (4), 5764−5783.
(23) Smith, G.; Kalli, K.; Sugden, K. *Advances in Femtosecond Micromachining and Inscription of Micro and Nano Photonic Devices, in Frontiers in Guided Wave Optics and Optoelectronics;* IntechOpen, 2010.
(24) Xu, Y.; Wang, R.; Ma, S.; Zhou, L.; Shen, Y.; Tian, C. Theoretical Analysis and Simulation of Pulsed Laser Heating at Interface. *J. Appl. Phys.* **2018**, *123* (2), No. 025301.
(25) Takai, K.; Tsujimura, S.; Kang, F.; Inagaki, M. *Graphene: Preparations, Properties, Applications and Prospects,* 1st ed.; Elsevier, 2020.
(26) Zhang, F.; Cerkauskaite, A.; Drevinskas, R.; Kazansky, P. G.; Qiu, J. Microengineering of Optical Properties of GeO2 Glass by Ultrafast Laser Nanostructuring. *Adv. Opt. Mater.* **2017**, *5* (23), 1700342.
(27) Scholtz, L.; Ladanyi, L.; Mullerova, J. Influence of Surface Roughness on Optical Characteristics of Multilayer Solar Cells. *Adv. Electr. Electron. Eng.* **2015**, *12* (6), 631−638.
(28) Rabchinskii, M.; Dideikin, A.; Kirilenko, D.; Baidakova, M.; Shnitov, V.; Roth, F.; Konyakhin, S.; Besedina, N.; Pavlov, S.; Kuricyn, R.; Lebedeva, N.; Brunkov, P.; Vul', A. Facile Reduction of Graphene Oxide Suspensions and Films Using Glass Wafers. *Sci. Rep.* **2018**, *8*, 14154.
(29) Kumar, P.; Bardhan, N.; Tongay, S.; Wu, J.; Belcher, A.; Grossman, J. Scalable Enhancement of Graphene Oxide Properties by Thermally Driven Phase Transformation. *Nat. Chem.* **2014**, *6*, 151−1258.
(30) Nair, R.; Blake, P.; Grigorenko, A.; Novoselov, K.; Booth, T.; Stauber, T.; Peres, N.; Geim, A. Fine Structure Constant Defines Visual Transparency of Graphene. *Science* **2008**, *320* (5881), 1308.
(31) Ferrari, A.; Meyer, J.; Scardaci, V.; Casiraghi, C.; Lazzeri, M.; Mauri, F.; Piscanec, S.; Jiang, D.; Novoselov, K.; Roth, S.; Geim, A. Raman Spectrum of Graphene and Graphene Layers. *Phys. Rev. Lett.* **2006**, *97* (18), 187401.
(32) Wan, J.; Gu, F.; Bao, W.; Dai, J.; Shen, F.; Luo, W.; Han, X.; Urban, D.; Hu, L. Sodium-Ion Intercalated Transparent Conductors with Printed Reduced Graphene Oxide Networks. *Nano Lett.* **2015**, *15* (6), 3763.
(33) Wang, S.; Dong, Y.; He, C.; Gao, Y.; Jia, N.; Chen, Z.; Song, W. The Role of sp^2/sp^3 Hybrid Carbon Regulation in the Nonlinear Optical Properties of Graphene Oxide Materials. *RSC Adv.* **2017**, *7* (84), 33676−33687.
(34) Chen, L.; Xu, Z.; Li, J.; Zhou, B.; Shan, M.; Li, Y.; Liu, L.; Li, B.; Niu, J. Modifying Graphite Oxide Nanostructures in Various Media by High-Energy Irradiation. *RSC Adv.* **2014**, *4*, 1025−1031.
(35) Iucci, G.; Battocchio, C.; Dettin, M.; Ghezzo, F.; Polzonetti, G. An XPS Study on the Covalent Immobilization of Adhesion Peptides on a Glass Surface. *Solid State Sci.* **2010**, *12*, 1861−1865.
(36) Arul, R.; Oosterbeek, R. N.; Robertson, J.; Xu, G.; Jin, J.; Simpson, M. C. The Mechanism of Direct Laser Writing of Graphene Features into Graphene Oxide Films Involves Photoreduction and Thermally Assisted Structural Rearrangement. *Carbon* **2016**, *99*, 423−431.

https://doi.org/10.1021/acsanm.1c01807
ACS Appl. Nano Mater. 2021, 4, 9283−9292